Influence of Metal Deposition and Activation Method on the Structure and Performance of Carbon Nanotube Supported Palladium Catalysts

Wouter S. Lamme, Jovana Zečević, and Krijn P. de Jong*[a]

The effects of the metal deposition and activation methods on metal particle size and distribution were investigated for carbon nanotube supported Pd catalysts. The Pd precursor was loaded by incipient wetness impregnation, ion adsorption, and deposition precipitation and was activated by thermal treatment under a nitrogen atmosphere or in the liquid phase by reduction by formaldehyde or sodium borohydride. Regardless of the metal precursor loading method, activation under a N_2 atmosphere at 500 °C led to homogeneously distributed 4 nm Pd particles. Liquid-phase reduction by sodium borohydride provided a bimodal distribution with particle sizes of approximately 1 and >10 nm. A somewhat weaker reducing agent, formaldehyde, yielded particles approximately 1 nm in size. The activities of the catalysts for the hydrogenation of cinnamaldehyde correlated with the particle sizes.

Carbon supported palladium (Pd/C) catalysts are widely used for hydrogenation in the fine-chemicals industry. Numerous studies have been performed investigating the influence of the support material,[1–5] the surface functional groups of the support,[6,7] metal precursor,[2,8] and activation method[2,9–11] on the structure and activity of the final Pd/C catalyst. Ideally, the metal particles should have a narrow size distribution and be uniformly distributed across the support to arrive at increased activity and stability. However, particles are often distributed nonuniformly or the particle-size distributions are broad or multimodal.[12–14]

Carbon supports that are often used include activated carbon, carbon black, graphite, and carbon nanomaterials such as carbon nanofibers and carbon nanotubes (CNTs). In research, CNTs are of particular interest, as they have a well-defined structure with a rather uniform surface, high purity, and

no micropores. The structure and porosity are largely maintained even if they are exposed to aggressive media.[15,16] The well-defined structure of CNTs makes them suitable for analysis by transmission electron microscopy, with high contrast between the supported metal nanoparticles and the support. Although CNTs are relatively inert, functional groups can be introduced onto the surface by functionalization treatment such as liquid-phase oxidation (LPO) and gas-phase oxidation (GPO). Surface chemistry can have a strong influence on metal dispersion[6,17] and interactions between the metal and the support[7,18] and, thus, on the performance of Pd/C catalysts.[7,17,19]

Various metal deposition methods such as impregnation,[2] deposition precipitation,[3,6] deposition reduction,[20] ion adsorption,[21,22] and colloidal routes[7,23] have been studied. The deposited metal precursor is commonly reduced in the gas phase, and this typically yields well-distributed Pd nanoparticles.[24,25] However, as Pd/C catalysts are often used in the liquid phase,[26] performing activation in the liquid phase is highly desirable.

In this work, we systematically investigated the influence of the different metal deposition methods and subsequent activation methods with varying conditions thereof on the structure of Pd/CNT catalysts. The $(NH_3)_4Pd(NO_3)_2$ precursor was deposited from aqueous solution onto LPO-treated CNTs by incipient wetness impregnation (IWI), deposition precipitation (DP), or ion adsorption (IA) with a nominal Pd loading of 5.0–6.0 wt%. The deposited Pd precursor was converted into metallic Pd particles in the gas phase by thermal treatment under a N_2 atmosphere at 500 °C.[19] Catalyst precursors prepared by ion adsorption were also reduced in the liquid phase by sodium borohydride or formaldehyde, both known to act as reducing agents in the preparation of Pd/C catalysts,[9,10,24,27] with varying conditions such as rate of addition of the reducing agent, temperature, and atmosphere under which the addition is performed. Details on the deposition and reduction methods can be found in the Supporting Information.

As expected, ion adsorption followed by gas-phase activation under a N_2 atmosphere yielded uniformly distributed Pd particles with a unimodal particle-size distribution and an average size of approximately 5 nm (Figure 1a). Comparable structures of Pd/C catalysts were observed if the deposition method was IWI or DP (Figure S1 in the Supporting Information). Ion adsorption was chosen to investigate further and to compare liquid-phase to gas-phase activation. In contrast to N_2 activation, reduction by sodium borohydride led to a bimodal particle-size distribution with 1 nm Pd particles uniformly distributed across the CNT support and 50 nm Pd particles proba-

[a] W. S. Lamme, Dr. J. Zečević, Prof. Dr. K. P. de Jong
    Inorganic Chemistry and Catalysis
    Debye Institute for Nanomaterials Science
    Utrecht University
    Universiteitsweg 99, 3584 CG Utrecht (The Netherlands)
    E-mail: k.p.dejong@uu.nl

    Supporting Information and the ORCID identification number(s) for the author(s) of this article can be found under https://doi.org/10.1002/cctc.201701991.
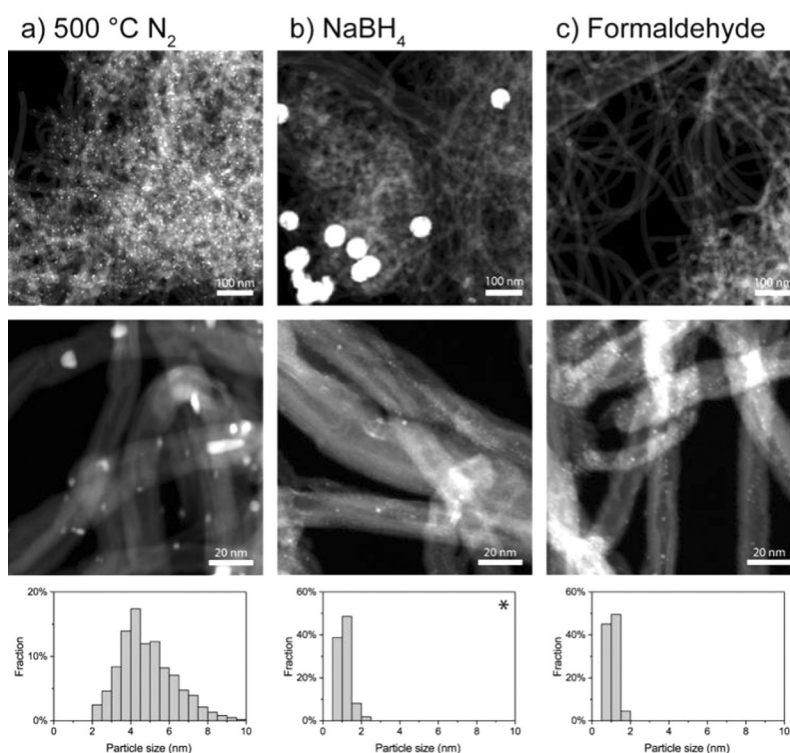
Figure 1. Representative high-angle annular dark-field scanning transmission electron microscopy (HAADF-STEM) images and particle-size distribution histograms of the Pd/CNT catalysts activated by a) thermal treatment at 500 °C under a N_2 atmosphere, b) slow addition of $NaBH_4$ at room temperature in air, c) instant addition of formaldehyde at room temperature under a N_2 atmosphere. Only sub-10 nm particles are included in the particle-size distribution of the $NaBH_4$-reduced sample.

bly located at the external surface of the CNT skeins (Figure 1 b).[28] Similarly, reduction by formaldehyde led to 1 nm Pd particles uniformly distributed over the support, but with only a negligible amount of the Pd ending up in 10–50 nm particles (Figure 1 c).

X-ray diffraction (XRD) and H_2 chemisorption were used to determine and compare the average Pd particle size from the bulk of a sample with that obtained by transmission electron microscopy (TEM) analysis (Table 1). Details on the characterization methods can be found in the Supporting Information. The ion-adsorption sample activated by N_2 treatment shows that the particle sizes determined by XRD, H_2 chemisorption, and TEM are similar. For the formaldehyde-reduced sample, the absence of Pd signals in the X-ray diffractograms and very low H_2 chemisorption-derived Pd particle sizes further corroborate that the 10–50 nm sized Pd particles observed by TEM are rather negligible. For the $NaBH_4$-reduced sample, the heteroge-

neity was quantified by calculating the contributions of the 1 and 50 nm particles to the average size determined by H_2 chemisorption. It was calculated that approximately 50 % of the Pd ended up as 1 nm particles and approximately 50 % of the Pd ended up as 50 nm particles.

One possible cause for the larger particles in the $NaBH_4$-reduced sample might be a higher loading of Pd in the sample. However, inductively coupled plasma (ICP) analysis confirmed that in all three ion-adsorption samples, as well as in all other samples prepared in this study, the achieved Pd loading was rather similar ranging from 3.7 to 4.4 wt % (see Table 1 and Table S1). Comparing the nominal loading of 5.0–6.0 wt % with the achieved loading of 3.7–4.5 wt % in the ion-adsorption samples, the extent of Pd deposition was approximately 70 %, which is slightly lower than the amounts of Pd deposited by IWI (85 %) and DP (95 %).

To investigate further how liquid-phase reduction might have affected the distribution of the metal nanoparticles over the support, experiments were performed under different atmospheres (air or N_2), different temperatures at which the reducing agent was added (RT and 2 and 80 °C), and different addition rates (fast or slow). Relative to the samples shown in Figure 1 b,c, none of the listed conditions seemed to impact the final catalyst structure significantly (Figures S2 and S3). The amount of $NaBH_4$ used also had no significant influence on the catalyst structure, as observed by TEM (Figure S2 f,g). Analysis of the metal loadings and Pd particle sizes determined by XRD, H_2 chemisorption, and TEM for all samples can be found in

Table 1. Weight loading, average crystallite sizes from XRD, and particle sizes from H_2 chemisorption and TEM.

Activation method	Pd loading [wt %]	Pd particle/crystallite size [nm]		
		XRD	H_2	TEM
N_2 treatment	4.0	2.6	3.6	3.2 ± 1.4
$NaBH_4$	4.4	2.9	2.0	$1/50^{[a]}$
formaldehyde	3.7	–	0.8	1.1 ± 0.3

[a] Bimodal distribution.

Table S1. These results exclude effects of concentration gradients as well as Ostwald ripening resulting from oxidation-reduction cycles.

An important difference between the NaBH$_4$-reduced and formaldehyde-reduced catalysts lies in the nature of the reducing agent. The standard reduction potentials (at pH 0) of Pd^{2+}/Pd, formic acid/formaldehyde, and boric acid/borohydride are 0.9, −0.25, and −0.5 V, respectively.[29–31] The more negative boric acid/borohydride potential may explain the observed differences by which the Pd particles grow to even 50 nm. This could be a result of immediate reduction of the metal precursor from the solution onto the support, whereas milder formaldehyde may reduce only precursor species adsorbed on the support.

All three catalysts were active in the hydrogenation of cinnamaldehyde (Table 2 and Figure S4). Normalized to the amount of Pd, the formaldehyde-reduced catalyst was much more active than the N$_2$-activated and NaBH$_4$-reduced catalysts. This difference could be explained by the particle sizes of the spent catalysts. The average particle sizes, determined by TEM, were (3.8 ± 1.4), (2.3 ± 1.3), and (2.0 ± 1.0) nm for the spent N$_2$-activated, NaBH$_4$-reduced (sub-10 nm particles only), and formaldehyde-reduced catalysts, respectively (Figure S6). The turnover frequencies calculated by using these sizes were similar.

Table 2. Catalytic activity and selectivity towards hydrocinnamyl aldehyde.

Activation method	Activity[a] [mmol g$_{Pd}^{-1}$ s^{-1}]	TOF[b] [s^{-1}]	Selectivity [%]
N$_2$ treatment	2.0	0.7	24
NaBH$_4$	2.4	1.0	63
formaldehyde	3.5	0.7	75

[a] Activity at 50% conversion, determined from a linear fit of ln($x_{cinnamaldehyde}$) versus t (see Figure S5). [b] Turnover frequency calculated as the number of cinnamaldehyde conversions per second, normalized to the number of Pd surface atoms calculated from the average Pd particle size of the spent catalysts, determined by TEM.

The selectivity to hydrocinnamaldehyde was 75% for the formaldehyde-reduced catalyst and 62% for the NaBH$_4$-reduced catalyst; the remaining amounts were hydrocinnamyl alcohol. A low selectivity of 24% was found for the N$_2$-activated catalyst. No cinnamyl alcohol was formed, as expected,[32] and no other products were observed in the GC traces. The difference in selectivity could be caused by the larger Pd particles in the NaBH$_4$-reduced sample.[33] Alternatively, the selectivity difference could be explained by support effects,[34] which could be introduced by a change in the nature of the functional groups caused by the activation method.

Preparation of Pd/CNT by using (NH$_3$)$_4$Pd(NO$_3$)$_2$ as a metal precursor and activation under a N$_2$ atmosphere yielded catalysts with particle sizes of approximately 4–5 nm distributed uniformly across the support regardless of the metal deposition method. Pd/CNT preparation by ion adsorption followed by reduction in the liquid phase by NaBH$_4$ yielded catalysts with a nonuniform metal-particle distribution and a bimodal

size distribution, whereas reduction by formaldehyde yielded a catalyst with uniformly distributed metal particles approximately 1 nm in size. Various liquid-phase reduction conditions appeared to have no influence on the final catalyst. It was the nature and probably the strength of the reducing agent that determined the final structure of the catalyst, with weaker reducing agents promoting narrower particle-size distributions and a uniform particle distribution across the support.

Acknowledgements

Conflict of interest

The authors declare no conflict of interest.

[1] V. M. Shinde, E. Skupien, M. Makkee, *Catal. Sci. Technol.* **2015**, *5*, 4144–4153.

[2] M. Gurrath, T. Kuretzky, H. P. Boehm, L. B. Okhlopkova, A. S. Lisitsyn, V. A. Likholobov, *Carbon* **2000**, *38*, 1241–1255.

[3] G. Agostini, E. Groppo, A. Piovano, R. Pellegrini, G. Leofanti, C. Lamberti, *Langmuir* **2010**, *26*, 11204–11211.

[4] R. M. Mironenko, O. B. Belskaya, T. I. Gulyaeva, A. I. Nizovskii, A. V. Kalinkin, V. I. Bukhtiyarov, A. V. Lavrenov, V. A. Likholobov, *Catal. Today* **2015**, *249*, 145–152.

[5] R. Pellegrini, G. Leofanti, G. Agostini, E. Groppo, M. Rivallan, C. Lamberti, *Langmuir* **2009**, *25*, 6476–6485.

[6] D. J. Suh, T.-J. Park, S.-K. Ihm, *Carbon* **1993**, *31*, 427–435.

[7] R. Arrigo, S. Wrabetz, M. E. Schuster, D. Wang, A. Villa, D. Rosenthal, F. Girsgdies, G. Weinberg, L. Prati, R. Schlögl, D. S. Su, *Phys. Chem. Chem. Phys.* **2012**, *14*, 10523–10532.

[8] M. Turáková, M. Králik, P. Lehocký, Ľ. Pikna, M. Smrčová, D. Remeteiová, A. Hudák, *Appl. Catal. A* **2014**, *476*, 103–112.

[9] A. Cabiac, G. Delahay, R. Durand, P. Trens, B. Coq, D. Plée, *Carbon* **2007**, *45*, 3–10.

[10] S. H. Jhung, J.-H. Lee, J.-M. Lee, J. H. Lee, D.-Y. Hong, M. W. Kim, J.-S. Chang, *Bull. Korean Chem. Soc.* **2005**, *26*, 563–568.

[11] G. Agostini, C. Lamberti, R. Pellegrini, G. Leofanti, F. Giannici, A. Longo, E. Groppo, *ACS Catal.* **2014**, *4*, 187–194.

[12] T. K. Das, S. Banerjee, M. Pandey, B. Vishwanadh, R. J. Kshirsagar, V. Sudarsan, *Int. J. Hydrogen Energy* **2017**, *42*, 8032–8041.

[13] B. Wang, T. Yan, T. Chang, J. Wei, Q. Zhou, S. Yang, T. Fang, *Carbon* **2017**, *122*, 9–18.

[14] S. Banerjee, K. Dasgupta, A. Kumar, P. Ruz, B. Vishwanadh, J. B. Joshi, V. Sudarsan, *Int. J. Hydrogen Energy* **2015**, *40*, 3268–3276.

[15] J.-P. Tessonnier, D. Rosenthal, T. W. Hansen, C. Hess, M. E. Schuster, R. Blume, F. Girsgdies, N. Pfänder, O. Timpe, D. S. Su, R. Schlögl, *Carbon* **2009**, *47*, 1779–1798.

[16] T. O. Eschemann, W. S. Lamme, R. L. Manchester, T. E. Parmentier, A. Cognigni, M. Rønning, K. P. De Jong, *J. Catal.* **2015**, *328*, 130–138.

[17] K. Chizari, I. Janowska, M. Houllé, I. Florea, O. Ersen, T. Romero, P. Bernhardt, M. J. Ledoux, C. Pham-Huu, *Appl. Catal. A* **2010**, *380*, 72–80.

[18] B. Zhang, L. Shao, W. Zhang, X. Sun, X. Pan, D. S. Su, *ChemCatChem* **2014**, *6*, 2607–2612.

[19] H. Markus, A. J. Plomp, P. Mäki-Arvela, J. H. Bitter, D. Y. Murzin, *Catal. Lett.* **2007**, *113*, 141–146.

[20] M. S. Hoogenraad, R. A. G. M. M. van Leeuwarden, G. J. B. van Breda Vriesman, A. Broersma, A. J. van Dillen, J. W. Geus, in *Prep. Catal. VI—Sci.*

Bases Prep. Heterog. Catal. Proc. Sixth Int. Symp. (Eds.: G. Poncelet, J. Martens, B. Delmon, P. Grange, P. A. Jacobs), Elsevier Science **1995**, pp. 263 – 271.

[21] A. Deffernez, S. Hermans, M. Devillers, *J. Phys. Chem. C* **2007**, *111*, 9448 – 9459.

[22] J. M. M. Tengco, Y. K. Lugo-José, J. R. Monnier, J. R. Regalbuto, *Catal. Today* **2015**, *246*, 9 – 14.

[23] P. T. Witte, P. H. Berben, S. Boland, E. H. Boymans, D. Vogt, J. W. Geus, J. G. Donkervoort, *Top. Catal.* **2012**, *55*, 505 – 511.

[24] A. Modak, A. Bhaumik, *J. Mol. Catal. A* **2016**, *425*, 147 – 156.

[25] M. L. Toebes, J. A. van Dillen, K. P. de Jong, *J. Mol. Catal. A* **2001**, *173*, 75 – 98.

[26] H.-U. Blaser, A. Indolese, A. Schnyder, H. Steiner, M. Studer, *J. Mol. Catal. A* **2001**, *173*, 3 – 18.

[27] S. Carrettin, P. McMorn, P. Johnston, K. Griffin, C. J. Kiely, G. J. Hutchings, *Phys. Chem. Chem. Phys.* **2003**, *5*, 1329 – 1336.

[28] M. Casavola, J. Hermannsdörfer, N. De Jonge, A. I. Dugulan, K. P. De Jong, *Adv. Funct. Mater.* **2015**, *25*, 5309 – 5319.

[29] W. H. Koppenol, J. D. Rush, *J. Phys. Chem.* **1987**, *91*, 4429 – 4430.

[30] *HSC Chemistry 7.14*, Outotec, Pori, **2009**.

[31] G. K. Schweitzer, L. L. Pesterfield, *The Aqueous Chemistry of the Elements*, Oxford University Press, **2010**.

[32] L. Zhang, J. M. Winterbottom, A. P. Boyes, S. Raymahasay, *J. Chem. Technol. Biotechnol.* **1998**, *72*, 264 – 272.

[33] F. Jiang, J. Cai, B. Liu, Y. Xu, X. Liu, *RSC Adv.* **2016**, *6*, 75541 – 75551.

[34] R. G. Rao, R. Blume, T. W. Hansen, E. Fuentes, K. Dreyer, S. Moldovan, O. Ersen, D. D. Hibbitts, Y. J. Chabal, R. Schlögl, J.-P. Tessonnier, *Nat. Commun.* **2017**, *8*, 340.